

Beyond the semiclassical approximation in atom interferometry

W. LaRow,¹ M. Edwards,² and C. A. Sackett^{1,*}

¹*Department of Physics, University of Virginia, Charlottesville, Virginia 22904, USA*

²*Department of Biochemistry, Chemistry and Physics,
Georgia Southern University, Statesboro, Georgia 30460, USA*

(Dated: January 15, 2025)

We describe a quantum perturbative approach to evaluating the phase shift of an atom interferometer in a weakly anharmonic trap. This provides a simple way to evaluate quantum corrections to the standard semi-classical approximation. The calculation benefits from the use of generalized coherent states for a basis. We find that the form of the semi-classical approximation remains valid to first order in the anharmonic perturbation, but that phase differences arise because the trajectory of a quantum wave packet will generally deviate from that of a classical particle. The quantum correction to the phase is a factor ℓ^2/A^2 smaller than the semi-classical perturbation itself, where ℓ is the quantum harmonic oscillator length scale and A is the classical amplitude of the motion. We provide analytical results for one-dimensional perturbations of power three through six in the position coordinate.

I. INTRODUCTION

Atom interferometry is a useful technique for precision measurements of a variety of phenomena [1, 2]. Generically, the sensitivity of an atom interferometer improves as its measurement time and spatial arm separations are increased. Although most atom interferometers use freely falling atoms, the large fall distance required for long interrogation times is an experimental challenge [3–7]. One solution is to use atoms confined in a trap, and recent experiments have demonstrated good performance with a variety of atom-trapping techniques [8–12].

We focus here on an approach using atoms confined in a harmonic trap, where they undergo linear or circular oscillations to make up the interferometer trajectory [10, 11, 13]. It is crucial in such experiments to understand the effect of the trapping potential itself on the interferometer phase. In principle this can be achieved through numerical solution of the Schrödinger or non-linear Schrödinger equation, as appropriate. However, numerical solution becomes impractical for sufficiently long measurement times and large arm separations. Advances in the technology of atom interferometry for precision measurements are pushing the field in precisely these directions, putting direct numerical solution of the Schrödinger and non-linear Schrödinger equations ever further out of reach.

An alternative tool that is useful in such situations is the semi-classical approximation (SCA) [14–21]. This assumes that the spatial extent of an atomic wave packet is negligibly small compared to the length scale over which the external potential varies, but large compared to the de Broglie wavelength of the propagating matter wave. The approximation is numerically tractable in most cases, and is simple enough to provide analytical results in some situations. The semiclassical method

is provably exact when the potential energy consists of terms of quadratic order or lower in the coordinates [14–16]. A harmonic trap satisfies this condition, but real traps will always include some anharmonicity. The main goal of this paper is to provide a first-order correction to the SCA for a trap with weak anharmonic contributions, so that the accuracy of the approximation can be easily assessed.

We find here that the semi-classical phase calculation does in fact remain accurate to first order in an anharmonic perturbation, as long as the semi-classical trajectory for a wave packet $x(t)$ is replaced by the quantum expectation value $\langle x \rangle(t)$. This expectation value will in general differ at first order from the semi-classical result, which does therefore cause a quantum correction to the phase. For non-interacting atoms, the leading correction is smaller than the SCA phase by a factor of order ℓ^2/A^2 , where ℓ is the quantum harmonic oscillator length scale and A is the classical amplitude of the motion.

This problem was also recently addressed by Glick and Kovachy [22], who developed a field-theoretic method based on Feynman diagrams. In comparison, our method uses elementary perturbation theory along with a generalized coherent state basis. The diagrammatic method is more general, applying equally to trapped and free-space interferometers and allowing for a larger class of perturbations. In contrast, our method more readily provides analytic low-order solutions for the trapped-atom configuration with power-law anharmonicity.

From an experimental perspective, the SCA has so far been satisfactory, and we are not aware of macro-scale atom interferometry measurements that demonstrate a need for quantum corrections. However, as measurement precision improves, we expect that quantum effects will play a significant role. We also suggest that there is a fundamental benefit in probing effects beyond the SCA as a test of quantum effects on a macroscopic scale. While the existence of matter-wave interference is in itself clearly non-classical, alternatives or generalizations of standard quantum mechanics [23, 24] might agree in

* sackett@virginia.edu

the semi-classical limit but differ in their predictions for quantum corrections.

The remainder of the paper is organized as follows: Section II develops a first-order approximation for the semi-classical phase, to which the quantum results will be compared. Section III uses quantum perturbation theory to analyze the interferometers. Section IV discusses the interpretation of the quantum results and some ways in which they can be extended. Finally, Section V provides a summary and points to some directions for future work.

II. SEMI-CLASSICAL PERTURBATION THEORY

A. The semi-classical approximation

We start with a summary of the conventional SCA for a light-pulse atom interferometer. In this approach, the measured phase difference θ is expressed as a sum of three terms [18]:

$$\theta_{SC} = \Delta\phi_{\text{prop}} + \Delta\phi_{\text{laser}} + \Delta\phi_{\text{sep}}. \quad (1)$$

The first is the dynamical propagation phase difference developed by the packets during their time evolution, where the phase for a single wave packet is given by

$$\phi_{\text{prop}} = \frac{1}{\hbar} \int_0^t [L(t') - E_{\text{int}}] dt'. \quad (2)$$

Here L is the classical Lagrangian $T - U$ evaluated along the classical trajectory $x(t)$, and E_{int} is the internal energy of the atom based on its quantum state. This expression conceptually follows from the path-integral formulation of quantum mechanics in which the phase associated with a possible trajectory is the the classical action divided by \hbar [14]; we can interpret the internal energy E_{int} as contributing to the classical potential energy U .

The laser term ϕ_{laser} comes from the interaction between an atomic wave packet and the laser pulses used to manipulate it. Every time a laser pulse imparts momentum $p = \hbar\kappa$ to a packet, the packet also acquires a phase

$$\phi_{\text{laser}} = \kappa x + \xi, \quad (3)$$

where x is the position of the packet at the time of the pulse and ξ is the phase of the laser field relative to an arbitrary fixed reference.

The separation phase occurs when the classical trajectories making up the interferometer do not perfectly intersect when the packets are recombined. If we consider each packet locally as a plane wave, then the phase gradient of the waves leads to a phase shift that depends on the packet separation,

$$\Delta\phi_{\text{sep}} = -\frac{m}{2\hbar}(v_{af} + v_{bf})(x_{bf} - x_{af}), \quad (4)$$

where x_{jf} and v_{jf} are the classical position and velocity for packet $j = a, b$ after the final interferometer light pulse. A non-zero final packet separation will generally lead to a reduction in the interferometer visibility as well, but the semi-classical approximation does not typically attempt to account for this.

B. Perturbative expansion

We apply the SCA method to the problem of an anharmonic oscillator. The atoms move in a one-dimensional potential

$$U(x) = \frac{1}{2}m\omega^2x^2 + V(x) \quad (5)$$

for small perturbation $V(x)$, and we take the internal energy to be zero. The atoms start at position x_i with velocity v_i , to which a laser pulse is applied to produce a superposition of states with momenta $mv_i + \hbar\kappa_{ai}$ and $mv_i + \hbar\kappa_{bi}$. The atoms evolve in the potential for time t , and are then recombined with momentum kicks $\hbar\kappa_{af}$ and $\hbar\kappa_{bf}$. We seek to evaluate the total SCA phase

$$\theta_{SC} = \phi_{\text{prop}, b} - \phi_{\text{prop}, a} + \phi_{\text{laser}, b} - \phi_{\text{laser}, a} + \Delta\phi_{\text{sep}}. \quad (6)$$

For the propagation phase terms, we evaluate the trajectories to first order in V by taking the position for arm $j = a, b$ to be $x_j(t) = x_{j0}(t) + x_{j1}(t)$, where x_{j0} is zeroth order in the perturbation and x_{j1} is first order. The various terms satisfy the classical equations of motion

$$\ddot{x} + \omega^2 x = -\frac{1}{m} \frac{dV}{dx} \quad (7a)$$

$$\ddot{x}_0 + \omega^2 x_0 = 0 \quad (7b)$$

$$\ddot{x}_1 + \omega^2 x_1 = -\frac{1}{m} \frac{dV}{dx} \bigg|_{x_0}. \quad (7c)$$

The initial conditions are included in x_0 , so $x_1(0) = \dot{x}_1(0) = 0$.

It will be convenient to express the interferometer phase in terms of the trajectory variables x_0 and x_1 . To this end, consider ϕ_{prop} for one wave packet:

$$\phi_{\text{prop}} = \frac{m}{2\hbar} \int_0^t (\dot{x}^2 - \omega^2 x^2) dt' - \frac{1}{\hbar} \int_0^t V(x) dt'. \quad (8)$$

In the first integral, integrate the \dot{x}^2 term by parts to obtain

$$\int_0^t \dot{x}^2 dt' = x\dot{x} \bigg|_0^t - \int_0^t \ddot{x}x dt'. \quad (9)$$

Then using (7a) to substitute for \ddot{x} and, approximating V to first order, we have

$$\begin{aligned} \phi_{\text{prop}} = & \frac{m}{2\hbar} [x(t)\dot{x}(t) - x(0)\dot{x}(0)] \\ & + \frac{1}{\hbar} \int_0^t \left[\frac{x_0}{2} \frac{dV}{dx} \bigg|_{x_0} - V(x_0) \right] dt'. \end{aligned} \quad (10)$$

Substitute from (7c) to relate

$$\int_0^t x_0 \frac{dV}{dx} \Big|_{x_0} dt' = -m \int_0^t x_0 (\ddot{x}_1 + \omega^2 x_1) dt'. \quad (11)$$

Integrating by parts twice yields

$$\int_0^t x_0 \ddot{x}_1 dt' = x_0 \dot{x}_1|_0^t - x_1 \dot{x}_0|_0^t + \int_0^t \ddot{x}_0 x_1 dt', \quad (12)$$

and then application of (7b) results in cancellation of the $\int \omega^2 x_0 x_1 dt$ term in (11). Using also the initial conditions for x_1 , we finally obtain

$$\begin{aligned} \phi_{\text{prop}} &= \frac{m}{2\hbar} [x(t)v(t) - x(0)v(0) - x_0(t)v_1(t) + x_1(t)v_0(t)] \\ &\quad - \frac{1}{\hbar} \int_0^t V(x_0) dt' \end{aligned} \quad (13)$$

where we relabel $\dot{x} \rightarrow v$.

To apply this result to the interferometer phase θ , we set $x_a(0) = x_i$ and $v_a(0) = v_i + \hbar \kappa_{ai}/m$, and abbreviate the final coordinates as $x_a(t) = x_a$, $v_a(t) = v_a$. This gives

$$\begin{aligned} \phi_{\text{prop},a} &= \frac{m}{2\hbar} (x_a v_a - x_i v_i - x_{a0} v_{a1} + x_{a1} v_{a0}) - \frac{1}{2} \kappa_{ai} x_i \\ &\quad - \frac{1}{\hbar} \int_0^t V[x_{a0}(t')] dt', \end{aligned} \quad (14)$$

with a similar expression for $\phi_{\text{prop},b}$. For the laser phase, we have

$$\phi_{\text{laser},b} - \phi_{\text{laser},a} = \kappa_{bi} x_i - \kappa_{ai} x_i + \kappa_{bf} x_b - \kappa_{af} x_a + \xi, \quad (15)$$

with $\xi \equiv \xi_b - \xi_a$ representing a phase shift of the recombination pulse. The separation phase is

$$\begin{aligned} \Delta\phi_{\text{sep}} &= -\frac{m}{2\hbar} \left(v_a + \frac{\hbar \kappa_{af}}{m} + v_b + \frac{\hbar \kappa_{bf}}{m} \right) (x_b - x_a) \\ &= \frac{m}{2\hbar} (x_a v_a - x_b v_b + x_a v_b - x_b v_a) \\ &\quad + \frac{1}{2} (\kappa_{af} x_a - \kappa_{bf} x_b + \kappa_{bf} x_a - \kappa_{af} x_b). \end{aligned} \quad (16)$$

Summing all these terms, we obtain

$$\begin{aligned} \theta_{SC} &= \xi + \frac{m}{2\hbar} (x_a v_b - x_b v_a) + \frac{1}{2} (\kappa_{bi} - \kappa_{ai}) x_i \\ &\quad + \frac{1}{2} (\kappa_{bf} - \kappa_{af}) (x_a + x_b) \\ &\quad + \frac{m}{2\hbar} [x_{b0} v_{b1} - x_{b1} v_{b0} - x_{a0} v_{a1} + x_{a1} v_{a0}] \\ &\quad - \frac{1}{\hbar} \int_0^t [V(x_{b0}) - V(x_{a0})] dt'. \end{aligned} \quad (17)$$

We can then separate out the perturbative orders, writing $\theta_{SC} = \theta_0 + \theta_1$ for

$$\begin{aligned} \theta_0 &= \xi + \frac{m}{2\hbar} (x_{a0} v_{b0} - x_{b0} v_{a0}) + \frac{1}{2} (\kappa_{bi} - \kappa_{ai}) x_i \\ &\quad + \frac{1}{2} (\kappa_{bf} - \kappa_{af}) (x_{a0} + x_{b0}) \end{aligned} \quad (18)$$

and

$$\begin{aligned} \theta_1 &= \frac{m}{2\hbar} [(v_{b0} - v_{a0})(x_{a1} + x_{b1}) - (v_{a1} + v_{b1})(x_{b0} - x_{a0})] \\ &\quad + \frac{1}{2} (\kappa_{bf} - \kappa_{af})(x_{a1} + x_{b1}) \\ &\quad - \frac{1}{\hbar} \int_0^t [V(x_{b0}) - V(x_{a0})] dt' \end{aligned} \quad (19)$$

In an experiment, the interferometer output would typically be detected by measuring the population P_f in the final momentum state, which varies as

$$P_f = \frac{1}{2} (1 + \mathcal{V} \cos \theta) \quad (20)$$

for visibility \mathcal{V} . The atomic contribution to θ could be determined by, for instance, scanning ξ to produce an interference fringe.

C. Cubic Potential

To illustrate the general results above, we apply them to a trap with cubic anharmonicity $V(x) = \beta x^3$. Although practical traps are more likely to exhibit perturbations with even powers of x , the asymmetry of the cubic potential means that its effects can be observed in a straightforward double-Bragg interferometer geometry, which simplifies the example here.

We consider an interferometer with atoms starting at rest at the trap center, $x_i = v_i = 0$. The atoms are split symmetrically with $\kappa_{ai} = -\kappa_{bi} = \kappa$, undergo nominally one half-period of oscillation with $\omega t = \pi$, and are then recombined to rest with $\kappa_{af} = -\kappa_{bf} = \kappa$. Solving the equations of motion (7) yields

$$x_{a0}(t) = A \sin \omega t \quad (21a)$$

$$x_{a1}(t) = -\frac{\beta A^2}{2m\omega^2} (3 - 4 \cos \omega t + \cos 2\omega t), \quad (21b)$$

where $A = \hbar \kappa / m \omega$ is the unperturbed amplitude of the motion. The result for x_b can be obtained by reversing the sign of A , so at $\omega t = \pi$ we have $x_{a0} = x_{b0} = 0$, $v_{a0} = -v_{b0} = -A\omega$, $x_{a1} = x_{b1} = -4\beta A^2 / m\omega^2$, and $v_{a1} = v_{b1} = 0$. We also have $\int_0^\pi \sin^3 u dt = 4/3$. Using these results, we find $\theta_0 = 0$ and the interferometer phase is

$$\theta_{SC} = \frac{8}{3} \frac{\beta A^3}{\hbar \omega}. \quad (22)$$

This arises entirely from the integral term in Eq. (19), since the terms involving $(v_{b0} - v_{a0})$ and $(\kappa_{bf} - \kappa_{af})$ cancel, while the $(v_{a1} + v_{b1})$ term is zero.

Figure 1 compares the results for the trajectory and phase to an exact numerical solution of the classical equations of motion. The perturbative result (22) correctly captures the leading dependence on β of the exact calculation.

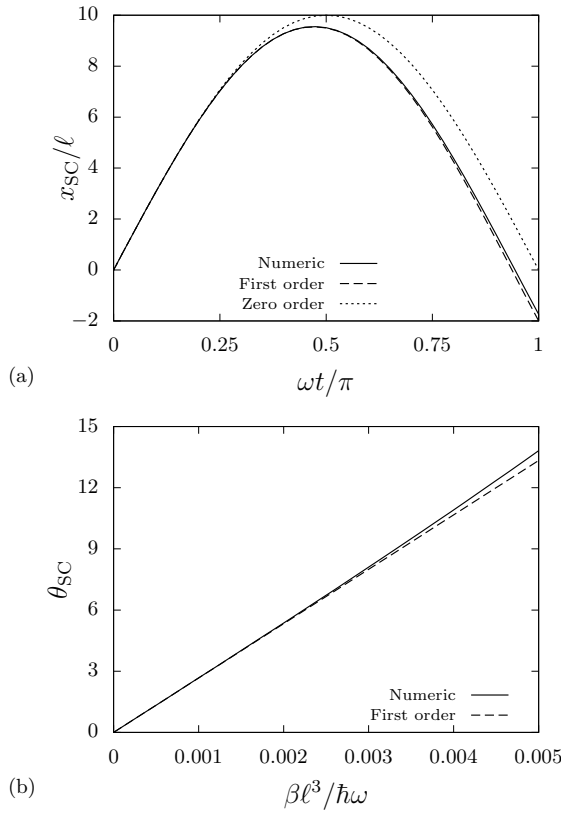


FIG. 1. Results of the semi-classical approximation for a symmetric interferometer in an anharmonic trap with perturbation $V(x) = \beta x^3$. Lengths are scaled by $\ell = \sqrt{\hbar/m\omega}$. (a) Trajectory of a classical particle starting with a velocity kick ωA for unperturbed oscillation amplitude $A = 10\ell$, with $\beta = 0.005\hbar\omega/\ell^3$. The solid line is a numerical solution of the exact equation of motion (7a). The dashed line is the perturbative result of Eq. (21). The dotted line shows the trajectory for the unperturbed oscillator, Eq. (21a), for comparison. (b) Interferometer phase θ_{SC} from the semi-classical approximation. The solid line shows the numerical solution, and the dashed line shows the perturbative result of (22).

III. QUANTUM PERTURBATIVE METHOD

A. General approach

We now seek to develop an analogous perturbative solution starting from a fully quantum description of the motion. We consider non-interacting atoms confined in a nearly harmonic potential, with Hamiltonian $H = H_0 + V(x)$ where

$$H_0 = \frac{p^2}{2m} + \frac{1}{2}m\omega^2x^2 \quad (23)$$

describes a harmonic oscillator and $V(x) \propto x^\lambda$ is a weak anharmonic perturbation that we assume to have power law form with integer $\lambda > 2$. Here we consider a one-dimensional system, but we discuss in Section IV how the technique might be extended to higher dimensions.

We also discuss there how mean-field interactions might be incorporated in an approximate way.

Our approach uses the standard formalism of time-dependent perturbation theory in the interaction picture [25]. The time-evolution of the Schrödinger-picture wavefunction is given by

$$\psi(t) = U_0(t)U_I(t)\psi(0), \quad (24)$$

where $U_0(t)$ is the unperturbed time-evolution operator $\exp(-iH_0t/\hbar)$ and $U_I(t)$ is the evolution operator in the interaction picture with respect to V . This satisfies the perturbation expansion

$$U_I(t) = 1 - \frac{i}{\hbar} \int_0^t dt_1 V_I(t_1) - \frac{1}{\hbar^2} \int_0^t dt_2 \int_0^{t_2} dt_1 V_I(t_2) V_I(t_1) + \dots, \quad (25)$$

where the perturbation in the interaction picture is

$$V_I(t) = U_0^\dagger(t)VU_0(t). \quad (26)$$

Our strategy is to express $\psi(t)$ in a basis of generalized coherent states, and then evaluate the effect of U_I using matrix mechanics.

B. Generalized coherent states

The generalized coherent (GC) states $|\alpha, n\rangle$ have seen occasional use in quantum optics contexts [26–28]. They are defined by

$$|\alpha, n\rangle = \hat{D}(\alpha)|n\rangle, \quad (27)$$

where $|n\rangle$ is the harmonic oscillator eigenstate with energy $(n + 1/2)\hbar\omega$ and $\hat{D}(\alpha)$ is the unitary displacement operator [29]

$$\hat{D}(\alpha) = e^{\alpha\hat{a}^\dagger - \alpha^*\hat{a}}. \quad (28)$$

Here \hat{a} and \hat{a}^\dagger are the usual harmonic oscillator ladder operators, and α is an arbitrary complex number. Conceptually, the GC state is a copy of the energy eigenstate $|n\rangle$ that oscillates in the harmonic potential with a complex amplitude proportional to α . For fixed α , the set $\{|\alpha, n\rangle\}$ forms a complete orthonormal basis [28] that we will use for the perturbation expansion.

The $|\alpha, 0\rangle$ state is identical to the ordinary coherent state $|\alpha\rangle$ satisfying $\hat{a}|\alpha\rangle = \alpha|\alpha\rangle$. To understand the action of \hat{a} on the generalized state $|\alpha, n\rangle$, use the commutator $[\hat{a}, \hat{D}(\alpha)] = \alpha D$ and thus

$$\begin{aligned} \hat{a}|\alpha, n\rangle &= \hat{a}\hat{D}(\alpha)|n\rangle = [\alpha\hat{D}(\alpha) + \hat{D}(\alpha)\hat{a}]|n\rangle \\ &= \alpha|\alpha, n\rangle + \sqrt{n}|\alpha, n-1\rangle. \end{aligned} \quad (29)$$

In a similar way,

$$\hat{a}^\dagger|\alpha, n\rangle = \alpha^*|\alpha, n\rangle + \sqrt{n+1}|\alpha, n+1\rangle. \quad (30)$$

With these, we obtain the action of the position operator,

$$\begin{aligned}\hat{x}|\alpha, n\rangle &= \frac{\ell}{\sqrt{2}} (\hat{a} + \hat{a}^\dagger) |\alpha, n\rangle \\ &= x_c |\alpha, n\rangle + \frac{\ell}{\sqrt{2}} [\sqrt{n} |\alpha, n-1\rangle + \sqrt{n+1} |\alpha, n+1\rangle],\end{aligned}\quad (31)$$

where $\ell \equiv \sqrt{\hbar/m\omega}$ and $x_c \equiv \sqrt{2}\ell \operatorname{Re} \alpha$. Noting that $\langle \alpha, m | \alpha, n \rangle = \delta_{mn}$, we see that the expectation value of the position is $\langle x \rangle = x_c$. We similarly find the action of the momentum operator

$$\begin{aligned}\hat{p}|\alpha, n\rangle &= mv_c |\alpha, n\rangle \\ &+ i \frac{m\omega\ell}{\sqrt{2}} [\sqrt{n+1} |\alpha, n+1\rangle - \sqrt{n} |\alpha, n-1\rangle].\end{aligned}\quad (32)$$

where $v_c \equiv \sqrt{2}\omega\ell \operatorname{Im} \alpha$ is the expectation value of the velocity.

The time evolution of the GC states follows from that of the eigenstates $|n\rangle$ and the operators \hat{a} , \hat{a}^\dagger . From $U_0(t)|n\rangle = e^{-i(n+1/2)\omega t}|n\rangle$ and $U_0(t)D(\alpha)U_0(-t) = D(\alpha e^{-i\omega t})$, we obtain

$$U_0(t)|\alpha, n\rangle = e^{-i(n+1/2)\omega t}|\alpha e^{-i\omega t}, n\rangle. \quad (33)$$

This time dependence for α means that the center position follows the classical trajectory $x_c(t) = x_c(0) \cos \omega t + [v_c(0)/\omega] \sin \omega t$ and that $v_c(t) = dx_c/dt$.

The spatial wave function $\psi_{\alpha,n}(x) \equiv \langle x | \alpha, n \rangle$ can be determined using the harmonic oscillator eigenstate wave functions and the translation properties of the displacement operator, yielding [26]

$$\begin{aligned}\psi_{\alpha,n}(x, t) &= \frac{\mathcal{A} e^{i\phi_c}}{\sqrt{2^n n!}} H_n \left(\sqrt{\frac{m\omega}{\hbar}} (x - x_c) \right) \\ &\times \exp \left[-\frac{m\omega(x - x_c)^2}{2\hbar} + i \frac{mv_c}{\hbar} (x - x_c) \right].\end{aligned}\quad (34)$$

Here $\mathcal{A} = (m\omega/\pi\hbar)^{1/4}$, H_n is the n th Hermite polynomial, and as above, $x_c = \sqrt{2}\ell \operatorname{Re} \alpha$ and $v_c = \sqrt{2}\ell \omega \operatorname{Im} \alpha$. The central phase $\phi_c = \arg[\psi(x_c)]$ is given by

$$\begin{aligned}\phi_c(t) &= \frac{m}{2\hbar} \left\{ x_c(0)v_c(0) + \int_0^t [v_c(t')^2 - \omega^2 x_c(t')^2] dt' \right\} \\ &- \left(n + \frac{1}{2} \right) \omega t.\end{aligned}\quad (35)$$

The time evolution of ϕ_c is consistent with the semi-classical propagation phase in Eq. (2), taking $E_{\text{int}} = (n + 1/2)\hbar\omega$. This correspondence is expected since the SCA is exact for a harmonic potential. As in the semi-classical calculation, the integral in (35) can be evaluated by parts to obtain the alternative form $\phi_c = mx_c(t)v_c(t)/2\hbar - (n + 1/2)\omega t$.

From Eq. (32) with $\hat{p} \rightarrow -i\hbar(\partial/\partial x)$, we can also obtain the derivative

$$\frac{\partial \psi_{\alpha,n}}{\partial x} = i \frac{mv_c}{\hbar} \psi_{\alpha,n} + \frac{1}{\sqrt{2}\ell} [\sqrt{n} \psi_{\alpha,n-1} - \sqrt{n+1} \psi_{\alpha,n+1}], \quad (36)$$

which will be used below. A final relation we require is

$$\langle \alpha, n | \beta, 0 \rangle = \langle \alpha | \beta \rangle \frac{(\beta - \alpha)^n}{\sqrt{n!}}, \quad (37)$$

where $\langle \alpha | \beta \rangle = \exp[-|\alpha - \beta|^2/2] \exp[(\alpha^* \beta - \beta^* \alpha)/2]$ is the overlap integral for standard coherent states. Result (37) is readily derived from Eq. (1.6) of Ref. [27].

C. First-order solution

Returning to the perturbation calculation, we take the initial state $|\psi(0)\rangle$ of the atoms to be the GC state $|\alpha_i, 0\rangle$, corresponding to a non-interacting Bose condensate that has potentially been displaced by a laser pulse. We express the subsequent evolution as a perturbation series

$$|\psi(t)\rangle = |\psi_0(t)\rangle + |\psi_1(t)\rangle + \dots \quad (38)$$

where $|\psi_\mu\rangle$ scales with V^μ . We have then

$$|\psi_0(t)\rangle = U_0(t)|\psi(0)\rangle = e^{-i\omega t/2}|\alpha(t), 0\rangle \quad (39)$$

for $\alpha(t) = \alpha_i e^{-i\omega t}$. We express the first-order correction as

$$|\psi_1(t)\rangle = \sum_n D_n(t) e^{-i\omega t/2} |\alpha(t), n\rangle \quad (40)$$

with coefficients

$$D_n = -\frac{i}{\hbar} e^{-in\omega t} \int_0^t dt_1 e^{i\omega n t_1} \langle \alpha(t_1), n | V | \alpha(t_1), 0 \rangle \quad (41)$$

following from Eq. (25).

The matrix elements in (41) are evaluated in closed form in the appendix, and are polynomials in the unperturbed position $x_c(t_1)$. The integrand in (41) thus involves products of sines and cosines in addition to the explicit complex exponential. These can always be integrated analytically, with examples provided in the appendix.

This method gives an expression for the wave function at time t . To relate to the semi-classical result, it is useful to evaluate the expectation values $\bar{x} \equiv \langle x \rangle$ and $\bar{v} \equiv \langle v \rangle$ for the position and velocity of the particle. To first order in V we have

$$\bar{x}(t) = \langle \psi | \hat{x} | \psi \rangle = x_c(t) + \sqrt{2}\ell \operatorname{Re} D_1(t), \quad (42)$$

and similarly

$$\bar{v}(t) = \frac{1}{m} \langle \psi | \hat{p} | \psi \rangle = v_c(t) + \sqrt{2}\ell \operatorname{Im} D_1(t). \quad (43)$$

We express these in perturbation orders as $\bar{x} = x_0 + x_1$ and $\bar{v} = v_0 + v_1$, identifying $x_0 = x_c = \sqrt{2\ell} \operatorname{Re} \alpha(t)$ and $v_0 = v_c = \sqrt{2\ell} \operatorname{Im} \alpha(t)$. Evidently, we can introduce a perturbed coherent state parameter

$$\bar{\alpha} = \alpha + D_1 = \frac{1}{\sqrt{2\ell}} \left(\bar{x} + i \frac{\bar{v}}{\omega} \right) \quad (44)$$

such that $|\bar{\alpha}\rangle$ gives the correct position and velocity for the perturbed evolution.

D. Interferometer analysis

Using the perturbation results, we consider the operation of an interferometer analogous to that of Section II. The initial coherent state is given by $\alpha_i = (x_i + iv_i/\omega)/\sqrt{2\ell}$. A laser pulse generates momentum kicks $\hbar\kappa_{ai}$ and $\hbar\kappa_{bi}$, to produce a superposition. The laser also imparts a phase shift; to model this, we take the effect of the laser as multiplication by $e^{i\kappa x}$, which from (34) and (35) results generally in

$$e^{i\kappa x} |\alpha, n\rangle = e^{i\kappa x_c/2} \left| \alpha + i\kappa\ell/\sqrt{2}, n \right\rangle. \quad (45)$$

The state after the beam-splitting operation is therefore

$$|\psi_i\rangle = \frac{1}{\sqrt{2}} \left[e^{i\kappa_{ai}x_i/2} |\alpha_{ai}, 0\rangle + e^{i\kappa_{bi}x_i/2} |\alpha_{bi}, 0\rangle \right], \quad (46)$$

for $\alpha_{ji} = [x_i + i(v_i + \kappa_{ji}\ell/\sqrt{2})/\omega]/\sqrt{2\ell}$ with $j = a, b$.

Each of the wave packets then evolves for time t such that, per Eq. (40),

$$|\alpha_{ji}, 0\rangle \rightarrow |\alpha_j, 0\rangle + \sum_n D_{jn} |\alpha_j, n\rangle. \quad (47)$$

Here we write D_{jn} for the D_n coefficient corresponding to packet j , and $\alpha_j = \alpha_{ji} e^{-i\omega t} \equiv (x_j + iv_j/\omega)/\sqrt{2\ell}$.

The laser is now applied again as a recombination pulse. We consider the final state $|\psi_f\rangle$ produced by applying laser kick κ_{af} to packet a with phase ξ_a , and kick κ_{bf} to packet b with phase ξ_b . The resulting state is

$$\begin{aligned} |\psi_f\rangle &= \frac{1}{2} \left[e^{i[(\kappa_{ai}x_i + \kappa_{af}x_a)/2 + \xi_a]} \left(|\alpha_{af}, 0\rangle + \sum_n D_{an} |\alpha_{af}, n\rangle \right) \right. \\ &\quad \left. + e^{i[(\kappa_{bi}x_i + \kappa_{bf}x_b)/2 + \xi_b]} \left(|\alpha_{bf}, 0\rangle + \sum_n D_{bn} |\alpha_{bf}, n\rangle \right) \right] \\ &\equiv \frac{1}{2} (|\psi_{af}\rangle + |\psi_{bf}\rangle), \end{aligned} \quad (48)$$

with $\alpha_{jf} = \alpha_j + i\kappa_{jf}\ell/\sqrt{2}$.

In some cases it is necessary to track the population in all final states, for instance if multiple interference paths can occur [30, 31]. For the simple interferometer considered here, however, we need only evaluate the population in state f , given by

$$\langle \psi_f | \psi_f \rangle = \frac{1}{4} [2 + \langle \psi_{af} | \psi_{bf} \rangle + \langle \psi_{bf} | \psi_{af} \rangle]. \quad (49)$$

Using Eq. (37) and expanding to first order in the perturbation, we have

$$\langle \psi_{af} | \psi_{bf} \rangle = e^{i[(\kappa_{bi}x_i + \kappa_{bf}x_b - \kappa_{ai}x_i - \kappa_{af}x_a)/2 + \xi]} \langle \alpha_{af} | \alpha_{bf} \rangle \left\{ 1 + \sum_n \frac{1}{\sqrt{n!}} [D_{an}^* (\alpha_{bf} - \alpha_{af})^n + D_{bn} (\alpha_{af}^* - \alpha_{bf}^*)^n] \right\}, \quad (50)$$

with $\xi = \xi_b - \xi_a$. In order to obtain interference, α_{af} and α_{bf} should be similar. We suppose $|\alpha_{af} - \alpha_{bf}| \ll 1$ and truncate the result to first order in this quantity. We can then also approximate

$$\langle \alpha_{af} | \alpha_{bf} \rangle \approx 1 + \frac{1}{2} (\alpha_{af}^* \alpha_{bf} - \alpha_{af} \alpha_{bf}^*) = 1 + \operatorname{Im}[\alpha_{af}^* \alpha_{bf}]. \quad (51)$$

The final population in (49) becomes $(1 + \cos \theta)/2$ with phase

$$\begin{aligned} \theta &= \xi + \frac{1}{2} (\kappa_{bi}x_i + \kappa_{bf}x_b - \kappa_{ai}x_i - \kappa_{af}x_a) \\ &\quad + \operatorname{Im}[\alpha_{af}^* \alpha_{bf}] + \operatorname{Im}[D_{a0}^* + D_{b0}] \\ &\quad + \operatorname{Im}[D_{a1}^* \alpha_{bf} - D_{a1}^* \alpha_{af} + D_{b1} \alpha_{af}^* - D_{b1} \alpha_{bf}^*]. \end{aligned} \quad (52)$$

The interferometer visibility here is equal to 1 because of the first-order approximation for $|\alpha_{bf} - \alpha_{af}|$.

To simplify the phase expression further, note that $\kappa x/2 = \operatorname{Im}(i\ell\kappa\alpha/\sqrt{2})$. If we also apply $\alpha_{jf} = \alpha_j +$

$i\kappa_{jf}\ell/\sqrt{2}$, we can express θ compactly as

$$\begin{aligned} \theta &= \operatorname{Im} \left[\bar{\alpha}_{af}^* \bar{\alpha}_{bf} + i\ell (\kappa_{bi}\alpha_i - \kappa_{ai}\alpha_i + \kappa_{bf}\bar{\alpha}_b - \kappa_{af}\bar{\alpha}_a) / \sqrt{2} \right. \\ &\quad \left. + D_{b0} - D_{a0} + D_{b1}^* \alpha_b - D_{a1}^* \alpha_a \right] + \xi, \end{aligned} \quad (53)$$

where we use the perturbed parameters of (44) with $\bar{\alpha}_j = \alpha_j + D_{j1}$ and $\bar{\alpha}_{jf} = \bar{\alpha}_j + i\kappa_{jf}\ell/\sqrt{2}$. We can also use Eq. (41) to express

$$\begin{aligned} \operatorname{Im} D_{j0} &= -\frac{1}{\hbar} \int_0^t \langle \alpha_j(t_1), 0 | V | \alpha_j(t_1), 0 \rangle dt' \\ &\equiv -\frac{1}{\hbar} \int_0^t \langle V \rangle_j dt' \end{aligned} \quad (54)$$

as the integral of the expectation value of the perturbation over the unperturbed trajectory. In this way, we obtain the final result in terms of position and velocity

parameters as

$$\begin{aligned} \theta = & \xi + \frac{m}{2\hbar}(\bar{x}_a\bar{v}_b - \bar{x}_b\bar{v}_a) + \frac{1}{2}(\kappa_{bi} - \kappa_{ai})x_i \\ & + \frac{1}{2}(\kappa_{bf} - \kappa_{af})(\bar{x}_a + \bar{x}_b) \\ & + \frac{m}{2\hbar}(x_{b1}v_{b0} - v_{b1}x_{b0} - x_{a1}v_{a0} + v_{a1}x_{a0}) \\ & - \frac{1}{\hbar} \int_0^t [\langle V \rangle_b - \langle V \rangle_a] dt'. \end{aligned} \quad (55)$$

Here we have set $\bar{\alpha}_j = (\bar{x}_j + i\bar{v}_j/\omega)/\sqrt{2\ell}$, $\alpha_j = (x_{j0} + iv_{j0}/\omega)/\sqrt{2\ell}$, and $D_{j1} = (x_{j1} + iv_{j1}/\omega)/\sqrt{2\ell}$, as respectively the total, zeroth-order, and first-order components of the quantum trajectory.

Notably, (55) has the same form as Eq. (17) from the SCA, if we identify the quantum expectation values \bar{x} , \bar{v} , and $\langle V \rangle$ with the classical variables x , v , and $V(x)$. In this sense, we conclude that the quantum result is consistent (to first order) with the semi-classical prescription (1). However, this does not mean that the semi-classical phase result is correct, because in general the quantum trajectory $\bar{x}(t)$ will differ from the classical $x(t)$, and $\langle V \rangle(t)$ differs from the classical $V(x(t))$. Ehrenfest's theorem [25] ensures that $m d\langle v \rangle/dt = -\langle dU/dx \rangle$ but if the potential U contains powers higher than quadratic, we do not generally have $\langle dU/dx \rangle = dU/d\langle x \rangle|_{\langle x \rangle}$. This difference is illustrated in the example below.

E. Evaluation for cubic anharmonicity

The method described above is applicable to any power law perturbation. We illustrate it here for a cubic anharmonicity $V(x) = \beta x^3$, as the simplest non-trivial example. We consider atoms starting with $x_i = 0$ and $v_i = A\omega$, for nominal oscillation amplitude A . Taking $x_c(t) = A \sin \omega t$, we use Eqs. (A.26) and (A.27) from the Appendix with $\tilde{x} = 0$ and $\tilde{v} = A/\ell$:

$$\begin{aligned} D_0 = & i \frac{\beta A}{\hbar \omega} \left[\frac{A^2}{12} (-8 + 9 \cos \omega t - \cos 3\omega t) \right. \\ & \left. - \frac{3}{2} \ell^2 (1 - \cos \omega t) \right] \end{aligned} \quad (56)$$

$$\begin{aligned} D_1 = & \frac{\beta \ell}{\sqrt{2} \hbar \omega} \left[\frac{A^2}{4} (-3e^{-2i\omega t} + 8e^{-i\omega t} - 6 + e^{2i\omega t}) \right. \\ & \left. + \frac{3}{2} \ell^2 (e^{-i\omega t} - 1) \right] \end{aligned} \quad (57)$$

The mean position is then

$$\begin{aligned} \bar{x} = & x_c + \sqrt{2\ell} \operatorname{Re} D_1 \\ = & A \sin \omega t - \frac{1}{2} \frac{\beta A^2}{m \omega^2} (3 - 4 \cos \omega t + \cos 2\omega t) \\ & - \frac{3}{2} \frac{\hbar \beta}{m^2 \omega^3} (1 - \cos \omega t). \end{aligned} \quad (58)$$

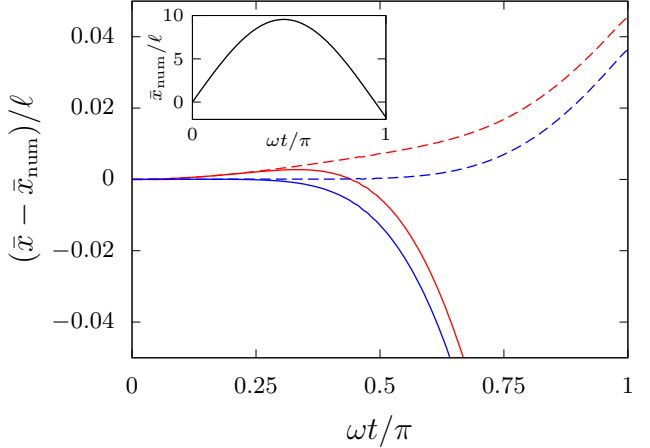


FIG. 2. (Color online) Trajectories $\bar{x}(t)$ in an anharmonic trap with perturbation $V = \beta x^3$, for $\beta = 0.005\hbar\omega/\ell^3$ and initial velocity $10\omega\ell$ with $\ell = \sqrt{\hbar/m\omega}$. The inset shows the expectation value \bar{x} calculated from exact numerical solution of the Schrödinger equation. The main plot shows the deviation from the exact result for the various approximations considered: the first-order semi-classical result (solid red), the second-order semi-classical result (red dashes), the first-order quantum perturbation result (solid blue), and the second-order quantum result (blue dashes).

Comparing to the semi-classical result of Eq. (21), we see there is an additional term representing the quantum correction to the motion.

Applying this result to a symmetric interferometer with $\kappa_{ai} = \kappa_{af} = -\kappa_{bi} = -\kappa_{bf} = m\omega A/\hbar$ and $\omega t = \pi$, we find from (55) that

$$\theta = \frac{8}{3} \frac{\beta A^3}{\hbar \omega} + 6 \frac{\beta A}{m \omega^2}. \quad (59)$$

Again the leading term for large A agrees with the semi-classical prediction of Eq. (22), but there is a quantum correction term that is smaller by a factor of order ℓ^2/A^2 .

We compare these results to both the semi-classical approximation and exact numerical solution of the Schrödinger equation. For the exact solution, we solve the Schrödinger equation using an explicit staggered-time algorithm [32]. Figure 2 shows the discrepancy between the $\langle x \rangle$ values from the numerical solution and the predictions of the first-order quantum perturbation calculations (solid blue) and SCA (solid red). It is evident that the quantum perturbation result remains accurate for longer. To better check the theory, we here carried out the perturbation calculations to second order (blue and red dashes). For this, evaluation of the perturbation matrix elements in Eq. (25) involves six applications of the \hat{x} operator at two different times, making the calculation less tractable. However, with the aid of Mathematica for symbolic manipulations, we obtained analytical results

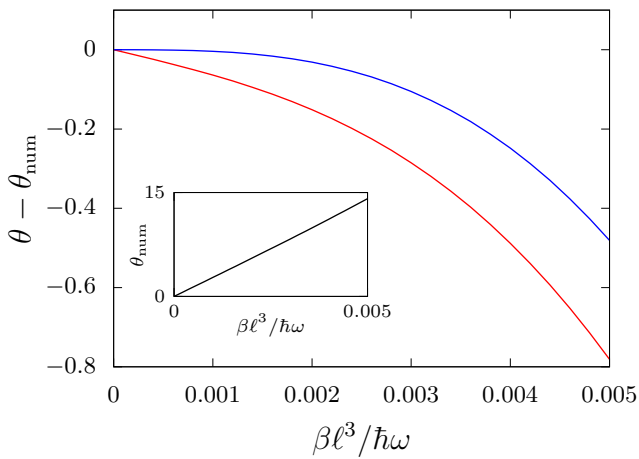


FIG. 3. (Color online) Interferometer phase θ for a symmetric interferometer in an anharmonic trap with perturbation $V = \beta x^3$, for packets with initial velocity $\pm 10\omega\ell$. The laser phase ξ is zero. The black curve is calculated using exact numerical solutions for the Schrödinger equation. The blue curve is the first-order quantum perturbation result of Eq. (59). The red curve is the first-order semi-classical result of (22).

for the second-order contributions to $\langle x \rangle$,

$$\begin{aligned} x_2 = & \frac{1}{16} \frac{\beta^2 A^3}{m^2 \omega^4} (-60\omega t \cos \omega t + 5 \sin \omega t \\ & + 32 \sin 2\omega t - 3 \sin 3\omega t) \\ & + \frac{5}{2} \frac{\beta^2 \hbar A}{m^3 \omega^5} (-3\omega t \cos \omega t + \sin \omega t + \sin 2\omega t). \end{aligned} \quad (60)$$

We emphasize the first-order results in our development as they are simpler and we expect the quantum corrections to be small in most practical situations, but the good agreement at second order does validate the GC method.

Figure 3 shows the exact and first-order approximations for the interferometer phase θ , as a function of β . The black curve is the exact result computed as $\arg(\langle \psi_a | \psi_b \rangle)$ where ψ_a and ψ_b are the final numerical wave functions for the two packets of the interferometer. The blue line shows the perturbative result of Eq. (59), and the red line shows the semi-classical result of (22). It is evident that the quantum perturbation result improves upon the semi-classical approximation.

IV. INTERPRETATION AND DISCUSSION

The parameters used in Figs. 2 and 3 were chosen to illustrate the quantum corrections in a regime where the exact Schrödinger equation is possible to solve numerically, enabling us to check the accuracy of the perturbation results. The calculations for Fig. 3 nonetheless took two hours to run using a fast algorithm on a

new desktop PC. The run time scales as $(A/\ell)^4$, which quickly becomes intractable as A increases. For example, in future experiments we hope to achieve $A = 300\ell$, corresponding to about 2 mm for Rb atoms in a 3-Hz trap. Numerical solution for these conditions would require substantial computational resources, and while this is perhaps achievable in one dimension, extension to three dimensions seems beyond reach. In contrast, the analytical method presented here can readily be extended to three-dimensions using a product GC basis $|\alpha_x, n_x\rangle |\alpha_y, n_y\rangle |\alpha_z, n_z\rangle$. As long as the analysis is restricted to first order, the effects of the perturbation on each degree of freedom can be analyzed independently and the results presented here can be directly applied.

For a realistic interferometer with multiple laser pulses, the wave function evolution must be evaluated in stages between pulses. The results derived here assume that the wave function at the start of a stage is a GC state with $n = 0$, which is not in general the case after the first stage. However, it is accurate at first order to replace the perturbed wave function $|\psi\rangle = |\psi_0\rangle + |\psi_1\rangle$ at the end of a stage with the displaced state $|\bar{\alpha}, 0\rangle$, using $\bar{\alpha}$ from Eq. (44). In this way, arbitrary interferometer sequences can be evaluated by the method presented here. Alternatively, the assumption that the initial quantum state has the form $|\alpha, 0\rangle$ can be relaxed. In that case, it would be necessary to consider more general matrix elements $\langle \alpha, n | V | \alpha, m \rangle$.

The results here are also useful for qualitative estimation. We see that the semi-classical component of the phase perturbation will generically be of order $\langle V \rangle / \hbar\omega$ where $\langle V \rangle$ is the average of the perturbation over the classical trajectory. The quantum correction to this phase correction will be smaller by a factor of order ℓ^2/A^2 , for classical amplitude A . For a perturbation $V \propto x^\lambda$, the quantum correction will scale as $A^{\lambda-2}$, so for $\lambda > 2$, the SCA becomes relatively more accurate as A becomes large, but the absolute size of the quantum correction increases without bound. As an example, the experiments of [13, 20] used ^{87}Rb atoms moving through a complicated trajectory in a trap with $\omega = 2\pi \times 3.5$ Hz and motional amplitude $A \approx 80\ell$. One relevant anharmonicity was quartic, $V = \beta_4 x^4$, with a coefficient $\beta_4 \approx (-2 \times 10^{-7}) \hbar\omega / \ell^4$. Without the need for a detailed calculation, we can estimate the semi-classical phase perturbation to be of order $\beta_4 A^4 / \hbar\omega \sim 10$ rad with a quantum correction of order $\beta_4 A^2 \ell^2 / \hbar\omega \approx 10^{-3}$ rad. This is small enough to neglect, but if the amplitude is increased to 300ℓ as proposed above, the corrections would become significant for a precision measurement. Interactions can also be expected to increase the quantum corrections, as discussed below.

The consistency between the quantum phase expression of Eq. (55) and the semi-classical result (17) suggests that the semi-classical idea is applicable even in the anharmonic case. This seems reasonable, since the path-integral formulation of quantum mechanics is itself valid for potentials of any form. It is worth noting, however,

that we cannot in general identify the propagation phase with the phase of the wave function at even the quantum-corrected position \bar{x} . From (55), we can subtract $\Delta\phi_{\text{laser}}$ and $\Delta\phi_{\text{sep}}$ to get an expression for the perturbed propagation phase on a given path,

$$\phi_{\text{prop}} = \frac{m}{2\hbar}(x_0 v_0 - x_i v_i + 2x_1 v_0) + \text{Im } D_0. \quad (61)$$

However, if we evaluate $\bar{\phi} \equiv \arg[\psi(\bar{x})]$, we obtain a different result. Using $\bar{x} = x_0 + x_1$ from Eq. (42), we expand

$$\psi(x_0 + x_1) \approx \psi_0(x_0) + x_1 \left. \frac{\partial \psi_0}{\partial x} \right|_{x_0} + \psi_1(x_0). \quad (62)$$

Since $x_0 = x_c$, the first and last terms can be evaluated using Eq. (34) as

$$\psi_0(x_0) = \mathcal{A}e^{i\phi_c} \quad \psi_1(x_0) = \mathcal{A}e^{i\phi_c} \sum_n h_n D_n, \quad (63)$$

where $\phi_c = (m/2\hbar)(x_0 v_0 - x_i v_i)$ is the central phase for the unperturbed system and the coefficients

$$h_n = \frac{H_n(0)}{\sqrt{2^n n!}} = \begin{cases} \left(-\frac{1}{2}\right)^{n/2} \binom{n}{n/2}^{1/2} & (n \text{ even}) \\ 0 & (n \text{ odd}) \end{cases} \quad (64)$$

come from $\psi_{\alpha,n}(x_c)$ in Eq. (34). The derivative term is evaluated with the aid of Eq. (36) as

$$\left. \frac{\partial \psi_0}{\partial x} \right|_{x_0} = i \frac{mv_0}{\hbar} \mathcal{A}e^{i\phi_c}. \quad (65)$$

These combine to give

$$\psi(\bar{x}) \approx \mathcal{A}e^{i\phi_c} \left[1 + i \frac{m}{\hbar} v_0 x_1 + \sum_{\text{even } n} h_n D_n \right]. \quad (66)$$

Interpreting the term in brackets as an expansion of $e^{i\phi_1}$, we obtain the central phase

$$\bar{\phi} = \frac{m}{2\hbar}(x_0 v_0 - x_i v_i + 2x_1 v_0) + \sum_{\text{even } n} h_n \text{Im } D_n. \quad (67)$$

This is similar to Eq. (61), but the sum includes terms with $n > 0$ that do not contribute to the interferometer phase. The validity of these terms was confirmed by comparison to numerical solution of the Schrödinger equation. We conclude that although the SCA concept remains useful for anharmonic systems, it is not possible to interpret the quantities involved as directly as in the harmonic case.

Another feature of our result is that the difference between the SCA and quantum phases is determined by the quantum corrections to the trajectory $\bar{x}(t)$ and expectation value $\langle V \rangle$. These corrections arise because the quantum wave function samples the perturbation over a range of values, and not just at a single classical point. In the case of the cubic perturbation, the quantum result can be recovered by replacing the classical potential

βx^3 with an effective potential averaged over a Gaussian wave function:

$$V_{\text{eff}}(x) = \frac{1}{\ell\sqrt{4\pi}} \int_{-\infty}^{\infty} e^{-(x-x')^2/\ell^2} \beta x'^3 dx' = \beta \left(x^3 + \frac{3}{2} \ell^2 x \right), \quad (68)$$

where the Gaussian corresponds to the probability distribution over x' of an ordinary coherent state centered at x . If we use this potential in the SCA calculation, we obtain agreement with the quantum results. However, for perturbations with power four or higher, this simple replacement does not suffice.

A more systematic way to approach this problem is with the Lagrangian Variational Method (LVM) [33, 34]. Here we suppose a trial wave function that depends on various parameters, and find equations of motion for those parameters by constructing an effective classical Lagrangian and applying the Euler-Lagrange technique. The calculation using V_{eff} above is equivalent to the LVM for a Gaussian trial wave function with x' as a variational parameter. In the case of a quartic perturbation, the quantum results can be recovered using a Gaussian where both the center and width are variational parameters. We plan to further explore this application of the LVM to atom interferometry in future work.

The effective potential or LVM approaches could also be useful for incorporating the effects of interactions into the phase calculation. An interacting condensate will typically have a Thomas-Fermi wave function with size $L \gg \ell$ [35]. Mean-field interactions can be included directly in the LVM Lagrangian, with the size L adopted as a variational parameter. Alternatively, an effective potential like V_{eff} can be defined using a Thomas-Fermi, rather than a Gaussian, probability distribution. For the purpose of estimation, it should normally be adequate to simply substitute $\ell \rightarrow L$ in the quantum perturbation results. For instance, the interferometer of [13] described above used condensates of about 2×10^4 atoms, which gives a Thomas-Fermi size $L \approx 3\ell$. The quantum correction to the anharmonic phase should therefore be estimated as $\beta_4 A^2 L^2 / \hbar\omega \approx 10^{-2}$ rad, about ten times larger than expected for the non-interacting case and already potentially significant.

V. SUMMARY AND FUTURE WORK

We have developed a quantum perturbation method appropriate for atom interferometers in nearly harmonic traps. Generalized coherent states provide an efficient basis for the calculation and lead to expressions for the required matrix elements that are easy to compute. We have shown that, at least to the first order of accuracy, the semi-classical approximation for phase estimation can be used in an anharmonic trap, but that the wave-packet trajectories are generally modified by quantum effects.

The quantum correction is generally smaller than the semi-classical result by a factor of ℓ^2/A^2 , where ℓ is the quantum harmonic oscillator length scale and A is the classical amplitude of motion.

This work raises a number of questions for further investigation. A notable one is whether and when the general semi-classical approach breaks down entirely, in the sense that propagation, laser, and separation phases cannot be usefully defined and evaluated. As a start, it would be interesting to extend the general result of Eq. (55) to second order and compare to the corresponding semi-classical expression. It may also be necessary to consider more carefully the light-atom interaction process: it is generally not accurate to treat the light field as an ideal plane wave [36–38], and as the size of a wave packet increases, the atoms will sample the optical deviations more strongly.

Another useful extension would be a method to evaluate the leading-order quantum correction to the phase while incorporating the exact classical motion. It is easy to envision practical situations where the anharmonicity is large enough that a perturbative expansion of the classical trajectory is inadequate, but at the same time the quantum corrections are small enough to approximate in first order. The effective potential and LVM approaches might be ways to achieve this goal, but it might also be possible to achieve a partial resummation of the quantum perturbation expansion (25) to express the classical part in all orders while retaining quantum corrections to the desired degree of accuracy.

It may also be possible to extend the analysis to situations more general than trapped atom interferometers with power-law perturbations. Free-space solutions can be obtained from our results in the limit $\omega \rightarrow 0$, but in that case the initial wave packet of an interferometer is not usually close to the ground state of the potential. Also, more general perturbations such as a localized ‘bump’ would typically lead to the coupling of many generalized coherent states, making our method inefficient. These situations might be more easily handled by diagrammatic methods [22].

In a practical direction, we hope to apply the techniques developed here to the three-dimensional interferometer configuration of [13], and in particular to evaluate the impact on the semi-classical results of [20]. The scaling analysis described above indicates that the quantum corrections will be fairly small, but large enough to be of potential significance in high-performance applications.

Finally, it would be interesting to measure a quantum correction effect in an interferometry experiment. For a trapped-atom experiment, our results suggest that the optimum configuration would use weak harmonic confinement (providing large ℓ) and a small amplitude of motion (low A), along with a relatively strong anharmonic perturbation to produce a measurable phase. We hope that the work presented here will stimulate efforts in this area.

ACKNOWLEDGMENTS

The authors gratefully acknowledge helpful conversations with Jonah Glick, Simon Haine, and Maxim Olshanii. We also thank Jeff Heward for help with the simulations. C.A.S. thanks the Quantum Science and Technology group at the Australian National University for hosting him while portions of this work were carried out. This work was supported by the National Science Foundation, Grant Nos. PHY-2110471 (C.A.S. and W.L.) and PHY-2207476 (M.E.).

Appendix

We here derive the coefficients D_n of Eq. (41), which can be expressed as

$$D_n = -\frac{i\beta_\lambda}{\hbar} e^{-in\omega t} \int_0^t e^{i\omega nt_1} f_n(t_1) dt_1 \quad (\text{A.1})$$

for matrix elements

$$f_n(t_1) = \langle \alpha(t_1), n | x^\lambda | \alpha(t_1), 0 \rangle \quad (\text{A.2})$$

with perturbation $V = \beta_\lambda x^\lambda$ and integer λ . We will first show that

$$f_n(t_1) = \frac{\eta}{\sqrt{n}} \frac{d}{dx_c} f_{n-1}(t_1), \quad (\text{A.3})$$

where $x_c = \eta[\alpha(t_1) + \alpha^*(t_1)]$ and $\eta = \ell/\sqrt{2} = \sqrt{\hbar/2m\omega}$. We then derive a general expression for f_0 , from which f_n can be obtained by differentiation.

To obtain (A.3) we start with

$$\langle \alpha, n | \hat{x}^\lambda | \alpha, 0 \rangle = \langle 0, n | \hat{D}^\dagger(\alpha) \hat{x}^\lambda \hat{D}(\alpha) | 0, 0 \rangle, \quad (\text{A.4})$$

and apply the displacement operator relation

$$\hat{D}^\dagger(\alpha) \hat{x}^\lambda \hat{D}(\alpha) = (\hat{x} + x_c)^\lambda. \quad (\text{A.5})$$

This gives

$$\begin{aligned} f_n &= \langle 0, n | (\hat{x} + x_c)^\lambda | 0, 0 \rangle \\ &= \frac{1}{\sqrt{n}} \langle n-1 | \hat{a} (\hat{x} + x_c)^\lambda | 0 \rangle \end{aligned} \quad (\text{A.6})$$

where $|0, n\rangle \equiv |n\rangle$ is the ordinary oscillator eigenstate and we have used $\langle n-1 | \hat{a} = \sqrt{n} \langle n |$. Since x_c is a scalar and $\hat{x} = \eta(\hat{a}^\dagger + \hat{a})$, we can expand

$$(\hat{x} + x_c)^\lambda = \sum_{k=0}^{\lambda} \binom{\lambda}{k} \eta^k x_c^{\lambda-k} (\hat{a}^\dagger + \hat{a})^k \quad (\text{A.7})$$

and obtain

$$f_n = \frac{1}{\sqrt{n}} \sum_{k=0}^{\lambda} \binom{\lambda}{k} \eta^k x_c^{\lambda-k} \langle n-1 | \hat{a} (\hat{a}^\dagger + \hat{a})^k | 0 \rangle. \quad (\text{A.8})$$

We now apply the commutator relation

$$[\hat{a}, (\hat{a} + \hat{a}^\dagger)^k] = k(\hat{a} + \hat{a}^\dagger)^{k-1} \quad (\text{A.9})$$

to see that

$$\langle n-1 | \hat{a} (\hat{a}^\dagger + \hat{a})^k | 0 \rangle = k \langle n-1 | (\hat{a} + \hat{a}^\dagger)^{k-1} | 0 \rangle \quad (\text{A.10})$$

since $\hat{a}|0\rangle = 0$. This then gives

$$f_n = \frac{1}{\sqrt{n}} \sum_{k=1}^{\lambda} \binom{\lambda}{k} k \eta^k x_c^{\lambda-k} \langle n-1 | (\hat{a}^\dagger + \hat{a})^{k-1} | 0 \rangle \quad (\text{A.11})$$

where we can start the sum at $k=1$ since the $k=0$ term is zero. Finally, we use the identities

$$\binom{\lambda}{k} k = \binom{\lambda}{k-1} (\lambda - k + 1) \quad (\text{A.12})$$

and

$$(\lambda - k + 1) \eta^k x_c^{\lambda-k} = \eta \frac{d}{dx_c} (\eta^{k-1} x_c^{\lambda-k+1}), \quad (\text{A.13})$$

to obtain

$$\begin{aligned} f_n &= \frac{\eta}{\sqrt{n}} \frac{d}{dx_c} \sum_{k=1}^{\lambda} \binom{\lambda}{k-1} \eta^{k-1} x_c^{\lambda-k+1} \langle n-1 | (\hat{a}^\dagger + \hat{a})^{k-1} | 0 \rangle \\ &= \frac{\eta}{\sqrt{n}} \frac{d}{dx_c} \sum_{k'=0}^{\lambda} \binom{\lambda}{k'} \eta^{k'} x_c^{\lambda-k'} \langle n-1 | (\hat{a}^\dagger + \hat{a})^{k'} | 0 \rangle \\ &= \frac{\eta}{\sqrt{n}} \frac{d}{dx_c} f_{n-1} \end{aligned} \quad (\text{A.14})$$

as desired. In the second equality above, we have shifted the summation index by setting $k' = k-1$ and extended the top summation limit from $k' = \lambda - 1$ to $k' = \lambda$. This does not change the value of the right-hand side because the $k' = \lambda$ term is independent of x_c and thus its derivative with respect to x_c is zero.

We now consider $f_0 = \langle \alpha, 0 | \hat{x}^\lambda | \alpha, 0 \rangle \equiv p_\lambda$. As above, we have

$$\begin{aligned} p_\lambda &= \langle 0 | (\hat{x} + x_c)^\lambda | 0 \rangle \\ &= \sum_{k=0}^{\lambda} \binom{\lambda}{k} \eta^k x_c^{\lambda-k} \langle 0 | (\hat{a} + \hat{a}^\dagger)^k | 0 \rangle. \end{aligned} \quad (\text{A.15})$$

Let us define

$$q_k = \langle 0 | (\hat{a} + \hat{a}^\dagger)^k | 0 \rangle. \quad (\text{A.16})$$

By parity, $q_k = 0$ for odd k , and it is easy to show that $q_0 = q_2 = 1$. We will derive a recursion relation for q_k .

We have

$$\begin{aligned} q_{k+2} &= \langle 0 | (\hat{a} + \hat{a}^\dagger)^2 (\hat{a} + \hat{a}^\dagger)^k | 0 \rangle \\ &= \langle 0 | (\hat{a}\hat{a} + \hat{a}\hat{a}^\dagger + \hat{a}^\dagger\hat{a} + \hat{a}^\dagger\hat{a}^\dagger) (\hat{a} + \hat{a}^\dagger)^k | 0 \rangle \end{aligned} \quad (\text{A.17})$$

Since $\langle 0 | \hat{a}^\dagger = 0$ and $\langle 0 | \hat{a}\hat{a}^\dagger = \langle 0 |$, (A.17) reduces to

$$q_{k+2} = \langle 0 | \hat{a}^2 (\hat{a} + \hat{a}^\dagger)^k | 0 \rangle + q_k. \quad (\text{A.18})$$

For the remaining term, use the commutator (A.9) twice, to get

$$\begin{aligned} q_{k+2} &= k(k-1) \langle 0 | (\hat{a} + \hat{a}^\dagger)^{k-2} | 0 \rangle + q_k \\ &= k(k-1) q_{k-2} + q_k. \end{aligned} \quad (\text{A.19})$$

This recursion, along with the q_0 and q_2 values, gives

$$q_k = (k-1)(k-3)\dots(1) = (k-1)!!.$$

Since k is even, we can use the identity

$$(k-1)!! = \frac{k!}{2^{k/2} (k/2)!}. \quad (\text{A.20})$$

Applying this to (A.15) and writing the binomial coefficient as factorials, we have

$$p_\lambda = \sum_{\text{even } k=0}^{\lambda} \frac{\lambda!}{2^{k/2} (k/2)! (\lambda-k)!} \eta^k x_c^{\lambda-k}, \quad (\text{A.21})$$

giving p_λ as a polynomial in x_c . Some results for relevant λ are

$$p_3(x_c) = x_c^3 + 3\eta^2 x_c \quad (\text{A.22})$$

$$p_4(x_c) = x_c^4 + 6\eta^2 x_c^2 + 3\eta^4 \quad (\text{A.23})$$

$$p_5(x_c) = x_c^5 + 10\eta^2 x_c^3 + 15\eta^4 x_c \quad (\text{A.24})$$

$$p_6(x_c) = x_c^6 + 15\eta^2 x_c^4 + 45\eta^4 x_c^2 + 15\eta^6 \quad (\text{A.25})$$

The coefficients $D_n(t)$ are obtained by first computing $f_n(t_1)$, and then integrating $e^{-i\omega t_1} f_n(t_1)$. In general, $x_c(t_1) = x_c(0) \cos(\omega t_1) + [v_c(0)/\omega] \sin(\omega t_1)$, so the integrals involve various products of $\sin \omega t_1$ and $\cos \omega t_1$. These can always be evaluated analytically using standard techniques. General results for $\lambda = 3$ to 6 are listed below, with the notation $D_{\lambda n} \equiv D_n$ for perturbation power λ and we use dimensionless variables $\tilde{x} = x_c(0)/\ell$, $\tilde{v} = v_c(0)/\omega \ell$:

$$\begin{aligned} D_{30}(t) &= \frac{i\beta_3 \ell^3}{12\hbar\omega} \left[-2\tilde{v}(9 + 4\tilde{v}^2 + 6\tilde{x}^2) + 9\tilde{v}(2 + \tilde{v}^2 + \tilde{x}^2) \cos \omega t - \tilde{v}(\tilde{v}^2 - 3\tilde{x}^2) \cos 3\omega t \right. \\ &\quad \left. - 9\tilde{x}(2 + \tilde{v}^2 + \tilde{x}^2) \sin \omega t + \tilde{x}(3\tilde{v}^2 - \tilde{x}^2) \sin 3\omega t \right] \end{aligned} \quad (\text{A.26})$$

$$D_{31}(t) = \frac{i\beta_3\ell^3}{4\sqrt{2}\hbar\omega} \left[-3(\tilde{v} - i\tilde{x})^2 e^{-2i\omega t} + 2(3 + 4\tilde{v}^2 - 4i\tilde{v}\tilde{x} + 2\tilde{x}^2)e^{-i\omega t} - 6(1 + \tilde{v}^2 + \tilde{x}^2) + (\tilde{v} + i\tilde{x})^2 e^{2i\omega t} \right] \quad (\text{A.27})$$

$$D_{40}(t) = -\frac{i\beta_4\ell^4}{32\hbar\omega} \left[4\tilde{v}\tilde{x}(12 + 3\tilde{v}^2 + 5\tilde{x}^2) + 12(2 + 4\tilde{v}^2 + 4\tilde{x}^2 + \tilde{v}^4 + 2\tilde{v}^2\tilde{x}^2 + \tilde{x}^4)\omega t - 16\tilde{v}\tilde{x}(3 + \tilde{v}^2 + \tilde{x}^2)\cos 2\omega t + 4\tilde{v}\tilde{x}(\tilde{v}^2 - \tilde{x}^2)\cos 4\omega t - 8(\tilde{v}^2 - \tilde{x}^2)(3 + \tilde{v}^2 + \tilde{x}^2)\sin 2\omega t + (\tilde{v}^4 - 6\tilde{v}^2\tilde{x}^2 + \tilde{x}^4)\sin 4\omega t \right] \quad (\text{A.28})$$

$$D_{41}(t) = -\frac{i\beta_4\ell^4}{8\sqrt{2}\hbar\omega} \left[2(\tilde{v} - i\tilde{x})^3 e^{-3i\omega t} + (12\tilde{v} + 12i\tilde{x} + 3\tilde{v}^3 + 9i\tilde{v}^2\tilde{x} + 15\tilde{v}\tilde{x}^2 + 5i\tilde{x}^3)e^{-i\omega t} + 12i(\tilde{v} - i\tilde{x})(2 + \tilde{v}^2 + \tilde{x}^2)\omega t e^{-i\omega t} - 6(\tilde{v} + i\tilde{x})(2 + \tilde{v}^2 + \tilde{x}^2)e^{i\omega t} + (\tilde{v} + i\tilde{x})^3 e^{3i\omega t} \right] \quad (\text{A.29})$$

$$D_{50}(t) = -\frac{i\beta_5\ell^5}{240\hbar\omega} \left[4\tilde{v}(225 + 200\tilde{v}^2 + 300\tilde{x}^2 + 32\tilde{v}^4 + 80\tilde{v}^2\tilde{x}^2 + 60\tilde{x}^4) - 150\tilde{v}(6 + 6\tilde{v}^2 + 6\tilde{x}^2 + \tilde{v}^4 + 2\tilde{v}^2\tilde{x}^2 + \tilde{x}^4)\cos \omega t + 25\tilde{v}(4\tilde{v}^2 - 12\tilde{x}^2 + \tilde{v}^4 - 2\tilde{v}^2\tilde{x}^2 - 3\tilde{x}^4)\cos 3\omega t - 3\tilde{v}(\tilde{v}^4 - 10\tilde{v}^2\tilde{x}^2 + 5\tilde{x}^4)\cos 5\omega t + 150\tilde{x}(6 + 6\tilde{v}^2 + 6\tilde{x}^2 + \tilde{v}^4 + 2\tilde{v}^2\tilde{x}^2 + \tilde{x}^4)\sin \omega t - 25\tilde{x}(12\tilde{v}^2 - 4\tilde{x}^2 + 3\tilde{v}^4 + 2\tilde{v}^2\tilde{x}^2 - \tilde{x}^4)\sin 3\omega t + 3\tilde{x}(5\tilde{v}^4 - 10\tilde{v}^2\tilde{x}^2 + \tilde{x}^4)\sin 5\omega t \right] \quad (\text{A.30})$$

$$D_{51}(t) = \frac{\beta_5\ell^5}{48\sqrt{2}\hbar\omega} \left[5(\tilde{v} - i\tilde{x})^4 e^{-4i\omega t} - 60(\tilde{v} - i\tilde{x})^2(3 + \tilde{v}^2 + \tilde{x}^2)e^{-2i\omega t} + 4(45 + 120\tilde{v}^2 - 120i\tilde{v}\tilde{x} + 60\tilde{x}^2 + 32\tilde{v}^4 - 32i\tilde{v}^3\tilde{x} + 48\tilde{v}^2\tilde{x}^2 - 48i\tilde{v}\tilde{x}^3 + 12\tilde{x}^4)e^{-i\omega t} - 90(2 + 4\tilde{v}^2 + 4\tilde{x}^2 + \tilde{v}^4 + 2\tilde{v}^2\tilde{x}^2 + \tilde{x}^4) + 20(\tilde{v} + i\tilde{x})^2(3 + \tilde{v}^2 + \tilde{x}^2)e^{2i\omega t} - 3(\tilde{v} + i\tilde{x})^4 e^{4i\omega t} \right] \quad (\text{A.31})$$

$$D_{60}(t) = -\frac{i\beta_6\ell^6}{192\hbar\omega} \left[4\tilde{v}\tilde{x}(270 + 135\tilde{v}^2 + 225\tilde{x}^2 + 15\tilde{v}^4 + 40\tilde{v}^2\tilde{x}^2 + 33\tilde{x}^4) + 60(6 + 18\tilde{v}^2 + 18\tilde{x}^2 + 9\tilde{v}^4 + 18\tilde{v}^2\tilde{x}^2 + 9\tilde{x}^4 + \tilde{v}^6 + 3\tilde{v}^4\tilde{x}^2 + 3\tilde{v}^2\tilde{x}^4 + \tilde{x}^6)\omega t - 90\tilde{v}\tilde{x}(12 + 8\tilde{v}^2 + 8\tilde{x}^2 + \tilde{v}^4 + 2\tilde{v}^2\tilde{x}^2 + \tilde{x}^4)\cos(2\omega t) + 36\tilde{v}\tilde{x}(\tilde{v}^2 - \tilde{x}^2)(5 + \tilde{v}^2 - \tilde{x}^2)\cos(4\omega t) - 2\tilde{v}\tilde{x}(3\tilde{v}^4 - 10\tilde{v}^2\tilde{x}^2 + 3\tilde{x}^4)\cos(6\omega t) - 45(\tilde{v}^2 - \tilde{x}^2)(12 + 8\tilde{v}^2 + 8\tilde{x}^2 + \tilde{v}^4 + 2\tilde{v}^2\tilde{x}^2 + \tilde{x}^4)\sin(2\omega t) + 9(5\tilde{v}^4 - 30\tilde{v}^2\tilde{x}^2 + 5\tilde{x}^4 + \tilde{v}^6 - 5\tilde{v}^4\tilde{x}^2 - 5\tilde{v}^2\tilde{x}^4 + \tilde{x}^6)\sin(4\omega t) - (\tilde{v}^2 - \tilde{x}^2)(\tilde{v}^4 - 15\tilde{v}^2\tilde{x}^2)\sin(6\omega t) \right] \quad (\text{A.32})$$

$$D_{61}(t) = \frac{i\beta_6\ell^6}{64\sqrt{2}\hbar\omega} \left[3(\tilde{v} - i\tilde{x})^5 e^{-5i\omega t} - 30(\tilde{v} - i\tilde{x})^3(4 + \tilde{v}^2 + \tilde{x}^2)e^{-3i\omega t} - 4(90\tilde{v} + 90i\tilde{x} + 45\tilde{v}^3 + 135i\tilde{v}^2\tilde{x} + 225\tilde{v}\tilde{x}^2 + 75i\tilde{x}^3 + 5\tilde{v}^5 + 25i\tilde{v}^4\tilde{x} + 40\tilde{v}^3\tilde{x}^2 + 40i\tilde{v}^2\tilde{x}^3 + 55\tilde{v}\tilde{x}^4 + 11i\tilde{x}^5)e^{-i\omega t} - 120i(\tilde{v} - i\tilde{x})(6 + 6\tilde{v}^2 + 6\tilde{x}^2 + \tilde{v}^4 + 2\tilde{v}^2\tilde{x}^2 + \tilde{x}^4)\omega t e^{-i\omega t} + 60(\tilde{v} + i\tilde{x})(6 + 6\tilde{v}^2 + 6\tilde{x}^2 + \tilde{v}^4 + 2\tilde{v}^2\tilde{x}^2 + \tilde{x}^4)e^{i\omega t} - 15(\tilde{v} + i\tilde{x})^3(4 + \tilde{v}^2 + \tilde{x}^2)e^{3i\omega t} + 2(\tilde{v} + i\tilde{x})^5 e^{5i\omega t} \right] \quad (\text{A.33})$$

tics and interferometry with atoms and molecules, *Rev. Mod. Phys.* **81**, 1051 (2009).

[3] L. Zhou, Z. Y. Xiong, W. Yang, B. Tang, W. C. Peng, K. Hao, R. B. Li, M. Liu, J. Wang, and M. S. Zhan, Development of an atom gravimeter and status of the 10-meter atom interferometer for precision gravity measurement, *Gen. Relativ. Gravit.* **43**, 1931 (2011).

[4] T. Kovachy, P. Asenbaum, C. Overstreet, C. A. Donnelly, S. M. Dickerson, A. Sugarbaker, J. M. Hogan, and M. A. Kasevich, Quantum superposition at the half-metre scale, *Nature* **528**, 530 (2015).

[5] B. Canuel, A. Bertoldi, L. Amand, E. Pozzo di Borgo, T. Chantrait, C. Danquigny, M. Dovale Álvarez, B. Fang, A. Freise, R. Geiger, J. Gillot, S. Henry, J. Hinderer, D. Holleville, J. Junca, G. Lefèvre, M. Merzougui, N. Mielec, T. Monfret, S. Pelisson, M. Prevedelli, S. Reynaud, I. Riou, Y. Rogister, S. Rosat, E. Cormier, A. Landragin, W. Chaibi, S. Gaffet, and P. Bouyer, Exploring gravity with the MIGA large scale atom interferometer, *Sci. Rep.* **8**, 10.1038/s41598-018-32165-z (2018).

[6] M.-S. Zhan, J. Wang, W.-T. Ni, D.-F. Gao, G. Wang, L.-X. He, R.-B. Li, L. Zhou, X. Chen, J.-Q. Zhong, B. Tang, Z.-W. Yao, L. Zhu, Z.-Y. Xiong, S.-B. Lu, G.-H. Yu, Q.-F. Cheng, M. Liu, Y.-R. Liang, P. Xu, X.-D. He, M. Ke, Z. Tan, and J. Luo, ZAIGA: Zhaoshan long-baseline atom interferometer gravitation antenna, *Int. J. Mod. Phys. D* **29**, 1940005 (2019).

[7] M. Abe, P. Adamson, M. Borcean, D. Bortolotto, K. Bridges, S. P. Carman, S. Chattopadhyay, J. Coleman, N. M. Curfman, K. DeRose, T. Deshpande, S. Dimopoulos, C. J. Foot, J. C. Frisch, B. E. Garber, S. Geer, V. Gibson, J. Glick, P. W. Graham, S. R. Hahn, R. Harnik, L. Hawkins, S. Hindley, J. M. Hogan, Y. Jiang, M. A. Kasevich, R. J. Kellett, M. Kiburg, T. Kovachy, J. D. Lykken, J. March-Russell, J. Mitchell, M. Murphy, M. Nantel, L. E. Nobrega, R. K. Plunkett, S. Rajendran, J. Rudolph, N. Sachdeva, M. Saifdari, J. K. Santucci, A. G. Schwartzman, I. Shipsey, H. Swan, L. R. Valerio, A. Vasonis, Y. Wang, and T. Wilkason, Matter-wave atomic gradiometer interferometric sensor (MAGIS-100), *Quantum Sci. and Technol.* **6**, 044003 (2021).

[8] C. Weidner and D. Z. Anderson, Experimental demonstration of shaken-lattice interferometry, *Phys. Rev. Lett.* **120**, 263201 (2018).

[9] V. Xu, M. Jaffe, C. D. Panda, S. L. Kristensen, L. W. Clark, and H. Müller, Probing gravity by holding atoms for 20 seconds, *Science* **366**, 745 (2019).

[10] E. R. Moan, R. A. Horne, T. Arpornthip, Z. Luo, A. J. Fallon, S. J. Berl, and C. A. Sackett, Quantum rotation sensing with dual Sagnac interferometers in an atom-optical waveguide, *Phys. Rev. Lett.* **124**, 120403 (2020).

[11] K. A. Krzyzanowska, J. Ferreras, C. Ryu, E. C. Samson, and M. G. Boshier, Matter-wave analog of a fiber-optic gyroscope, *Phys. Rev. A* **108**, 043305 (2023).

[12] Y. Balland, L. Absil, and F. Pereira Dos Santos, Queennewton local force sensor, *Phys. Rev. Lett.* **133**, 113403 (2024).

[13] M. M. Beydler, E. R. Moan, Z. Luo, Z. Chu, and C. A. Sackett, Guided-wave Sagnac atom interferometer with large area and multiple orbits, *AVS Quantum Sci.* **6**, 10.1116/5.0173769 (2024).

[14] P. Storey and C. Cohen-Tannoudji, The Feynman path integral approach to atomic interferometry. A tutorial, *J. Phys. II France* **4**, 1999 (1994).

[15] C. Antoine and C. J. Bordé, Quantum theory of atomic clocks and gravito-inertial sensors: an update, *J. Opt. B: Quantum Semiclass. Opt.* **5**, S199 (2003).

[16] C. Antoine and C. Bordé, Exact phase shifts for atom interferometry, *Phys. Lett. A* **306**, 277 (2003).

[17] K. Bongs, R. Launay, and M. Kasevich, High-order inertial phase shifts for time-domain atom interferometers, *Appl. Phys. B* **84**, 599 (2006).

[18] J. M. Hogan, D. M. S. Johnson, and M. A. Kasevich, Light-pulse atom interferometry, in *Atom Optics and Space Physics*, Proceedings of the International School of Physics “Enrico Fermi”, Vol. 168 (IOS Press, Amsterdam, 2009) pp. 411–447.

[19] G. M. Tino and M. A. Kasevich, eds., *Atom Interferometry*, Proceedings of the International School of Physics “Enrico Fermi”, Vol. 188 (IOS Press, Amsterdam, 2014).

[20] Z. Luo, E. R. Moan, and C. A. Sackett, Semiclassical phase analysis for a trapped-atom Sagnac interferometer, *Atoms* **9**, 21 (2021).

[21] C. Overstreet, P. Asenbaum, and M. A. Kasevich, Physically significant phase shifts in matter-wave interferometry, *Am. J. Phys.* **89**, 324 (2021).

[22] J. Glick and T. Kovachy, Feynman diagrams for matter wave interferometry (2024), arXiv:2407.11446 [physics.atom-ph].

[23] A. Bassi, K. Lochan, S. Satin, T. P. Singh, and H. Ulbricht, Models of wave-function collapse, underlying theories, and experimental tests, *Rev. Mod. Phys.* **85**, 471 (2013).

[24] B. L. B. Hu and E. Verdaguer, *Semiclassical and Stochastic Gravity: Quantum Field Effects on Curved Spacetime*, Cambridge Monographs on Mathematical Physics (Cambridge University Press, Cambridge, 2020).

[25] R. Shankar, *Principles of Quantum Mechanics*, 2nd ed. (Springer, New York, 1994).

[26] I. R. Senitzky, Harmonic oscillator wave functions, *Phys. Rev.* **95**, 1115 (1954).

[27] M. Boiteux and A. Levelut, Semicohherent states, *J. Phys. A: Math. Nucl. Gen.* **6**, 589 (1973).

[28] T. G. Philbin, Generalized coherent states, *Am. J. Phys.* **82**, 742 (2014).

[29] L. Mandel and E. Wolf, *Optical coherence and quantum optics* (Cambridge University Press, New York, 1995).

[30] M. Weitz, T. Heupel, and T. W. Hänsch, Multiple beam atomic interferometer, *Phys. Rev. Lett.* **77**, 2356 (1996).

[31] S.-B. Lu, Z.-W. Yao, R.-B. Li, J. Luo, S. Barthwal, H.-H. Chen, Z.-X. Lu, J. Wang, and M.-S. Zhan, Competition effects of multiple quantum paths in an atom interferometer, *Opt. Comm.* **429**, 158 (2018).

[32] P. B. Visscher, A fast explicit algorithm for the time-dependent Schrödinger equation, *Comput. Phys.* **5**, 596 (1991).

[33] V. M. Pérez-García, H. Michinel, J. I. Cirac, M. Lewenstein, and P. Zoller, Low energy excitations of a Bose-Einstein condensate: A time-dependent variational analysis, *Phys. Rev. Lett.* **77**, 5320 (1996).

[34] S. Thomas, C. Sapp, C. Henry, A. Smith, C. A. Sackett, C. W. Clark, and M. Edwards, Modeling atom interferometry experiments with Bose-Einstein condensates in power-law potentials, *Atoms* **10**, 34 (2022).

[35] F. Dalfovo, S. Giorgini, L. Pitaevskii, and S. Stringari, Theory of Bose-Einstein condensation in trapped gases, *Rev. Mod. Phys.* **71**, 463 (1999).

- [36] A. Louchet-Chauvet, T. Farah, Q. Bodart, A. Clairon, A. Landragin, S. Merlet, and F. P. D. Santos, The influence of transverse motion within an atomic gravimeter, *New J. Phys.* **13**, 065025 (2011).
- [37] V. Schkolnik, B. Leykauf, M. Hauth, C. Freier, and A. Peters, The effect of wavefront aberrations in atom interferometry, *Appl. Phys. B* **120**, 311 (2015).
- [38] M.-K. Zhou, Q. Luo, L.-L. Chen, X.-C. Duan, and Z.-K. Hu, Observing the effect of wave-front aberrations in an atom interferometer by modulating the diameter of Raman beams, *Phys. Rev. A* **93**, 043610 (2016).